

Influenza transmission in the guinea pig model is insensitive to the ventilation airflow speed: Evidence for the role of aerosolized fomites

Sima Asadi ^{1,*}, Nassima Gaaloul ben Hnia,² Ramya S. Barre ^{2,†}, Anthony S. Wexler ^{3,4,5,6},
William D. Ristenpart ^{1,‡} and Nicole M. Bouvier ^{2,7}

¹Department of Chemical Engineering, University of California Davis, 1 Shields Ave.,
Davis, California 95616, USA

²Department of Microbiology, Icahn School of Medicine at Mount Sinai, 1 Gustave L. Levy Place,
New York, New York 10029, USA

³Department of Mechanical and Aerospace Engineering, University of California Davis,
1 Shields Ave., Davis, California 95616, USA

⁴Air Quality Research Center, University of California Davis, 1 Shields Ave., Davis, California 95616, USA

⁵Department of Civil and Environmental Engineering, University of California Davis,
1 Shields Ave., Davis, California 95616, USA

⁶Department of Land, Air and Water Resources, University of California Davis,
1 Shields Ave., Davis, California 95616, USA

⁷Department of Medicine, Division of Infectious Diseases, Icahn School of Medicine at Mount Sinai,
1 Gustave L. Levy Place, New York, New York 10029, USA



(Received 29 June 2021; accepted 13 December 2022; published 20 April 2023)

Recent experimental work in a guinea pig model has established that influenza A virus is transmissible through the air via aerosolized fomites, which are microscopic dust and dander particulates contaminated with infectious virus [S. Asadi *et al.*, *Nat. Commun.* **11**, 4062 (2020)]. Here we report that influenza A transmits efficiently from intranasally inoculated animals to downwind susceptible animals over a wide range of ventilation airspeeds with no statistically significant change in transmission probability despite increasing the airspeed by a factor of ten. We demonstrate that this finding is inconsistent with a transmission mechanism predicated entirely on emission of virus-laden expiratory particles from the inoculated animal, since the resulting airborne viral concentrations should be greatly diluted at larger airspeeds. Instead, the results suggest that the overall rate of virus aerosolization increases with the ventilation airspeed, in accord with a transmission mechanism predicated on aerosolized fomites in which their generation rate is proportional to the airspeed.

DOI: [10.1103/PhysRevFluids.8.040502](https://doi.org/10.1103/PhysRevFluids.8.040502)

*Present address: Department of Chemical Engineering, Massachusetts Institute of Technology, 77 Massachusetts Ave., Cambridge, MA 02139, USA.

†Present address: Department of Microbiology, Immunology, and Molecular Genetics, University of Texas Health Science Center at San Antonio, San Antonio, TX 78229, USA.

‡Corresponding author: wristenpart@ucdavis.edu

Published by the American Physical Society under the terms of the [Creative Commons Attribution 4.0 International](https://creativecommons.org/licenses/by/4.0/) license. Further distribution of this work must maintain attribution to the author(s) and the published article's title, journal citation, and DOI.

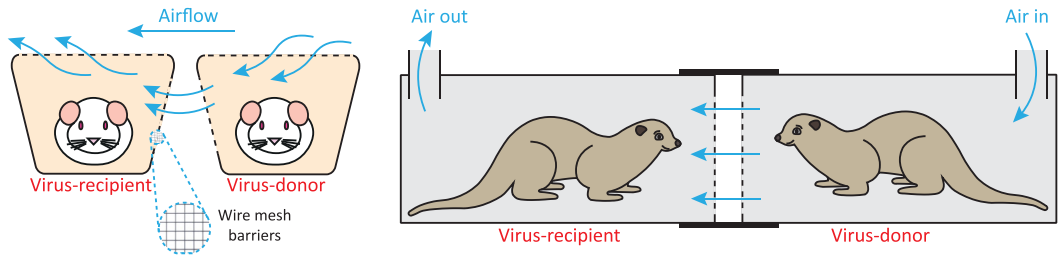


FIG. 1. Examples of traditional airborne transmission experiment setups. A virus-donor animal (a guinea pig or a ferret) is placed in a cage downstream from a virus-recipient animal in a separated cage. The animals do not have direct contact with each other, but the air can be exchanged between two cages via openings created on cage walls and covered with wire mesh barriers (dashed lines).

I. INTRODUCTION

The ongoing COVID-19 pandemic has highlighted large knowledge gaps in how respiratory viruses spread through the air between humans [1–3]. Virus-containing respiratory droplets, emitted when infected individuals breathe, speak, sing, sneeze, or cough, are commonly assumed to carry viruses through the air to new susceptible human hosts [4–8]. Direct corroboration of this assumption is challenging to perform experimentally with humans, however, so researchers often turn to animal models to investigate airborne virus transmissibility under controlled laboratory conditions to investigate airborne virus transmissibility. In this approach, a “virus-donor” animal, for example a guinea pig [9–11] or a ferret [12,13], is inoculated with a respiratory virus, and a “virus-recipient” animal, naive to virus and thus susceptible to transmitted infection, is physically separated from the virus-donor animal. Cages are configured so that the donor and recipient animals share a common air space but are prevented from direct contact with one another (Fig. 1). Thus, if the susceptible animal becomes infected, it is assumed that virus emitted from the respiratory tract of the infected donor, carried either in large-droplet sprays or in small aerosol particles, traveled through the air to infect the recipient animal. Thus, the viral load in respiratory tract of the donor animal—essentially, the reservoir of viable virus particles from which the recipient animal is infected by transmission—is typically quantified by titrating viable virus from nasal wash or nasopharyngeal swab samples [14,15]. This basic experimental framework is regularly used to test seasonal zoonotic viral strains for airborne transmissibility [10,12] and to perform more fundamental work such as identifying specific mutations necessary to render particular strains of influenza to be airborne transmissible [16]. Likewise, researchers are now rushing to understand airborne transmission of SARS-CoV-2 in animal models [17–19].

Although these transmission experiments confirm whether a virus is airborne transmissible, they do not tell you *what type of airborne particulate matter* actually carried the virus to the susceptible recipient animal. The usual assumption in influenza virus transmission research has been that expiratory droplets or aerosols emitted from the respiratory tract of the inoculated animal carry the virus, but nothing about this experimental configuration guarantees that this is what occurs. In fact, recent experimental work by Asadi *et al.* with a guinea pig model directly established that “aerosolized fomites” from virus-contaminated animals could transmit influenza through the air [20]. Tests with intranasally inoculated guinea pigs confirmed that they heavily contaminated their fur and their cage environment, presumably via self-grooming and direct contact with their environment. In regard to transmission, Asadi *et al.* showed that virus-immune donor animals whose bodies were purposely contaminated with influenza virus could transmit influenza through the air to virus-naive animals, even though the donor animals had no measurable virus in their respiratory tract. Separate *in vitro* tests confirmed that viable aerosolized fomites could even be released from inanimate sources like virus-contaminated paper tissues. Further work with a laser interferometry apparatus [21] demonstrated that the vast majority of micron-scale airborne particles moving from

one cage to the other were actually aerosolized dust, not respiratory droplets; despite much effort, no clearly liquid droplets were ever observed exiting from the guinea pig cages. Taken together, the results indicate that some unknown percentage of airborne influenza transmission in animal models could be due to aerosolized fomites rather than entirely due to expiratory droplets, as is commonly assumed.

Given this uncertainty, and given the importance of animal models in evaluating airborne disease transmission, a fundamental understanding of how the virus actually travels from the donor animal to the susceptible animal is paramount. To our knowledge, however, there are no known techniques for directly determining whether an expiratory droplet or an aerosolized fomite is what actually carried the virus from an infected donor animal to a recipient susceptible animal. The prior work by Asadi *et al.* established that transmission via aerosolized fomites can occur from immune but contaminated animals that do not emit virus-laden respiratory particles, but it is difficult or impossible to perform the converse experiment, in which animals emit virus-laden respiratory particles but do not produce aerosolized fomites. Typical transmission experiments involve exposure times of several days, during which it is ethically challenging to restrain donor animals from self-grooming or otherwise contaminating their environment and to eliminate the fur, food, or bedding that are sources of microscopic particulates to be contaminated. Stationary, anesthetized guinea pigs almost completely covered in a metal enclosure to minimize dust aerosolization nonetheless emitted micron-scale particulates at rates almost identical to euthanized guinea pigs [20]. In other words, even motionless, nonbreathing animals emit dust particulates that could potentially be aerosolized fomites. It is unclear how one could directly test whether expiratory droplets or aerosolized fomites were responsible for carrying the virus from an infected animal in a transmission experiment.

Instead, we turn to indirect techniques. A fundamental aspect of airborne transmission in animal models is that the virus, regardless of whether it is carried in an expiratory droplet or on an aerosolized fomite, necessarily moves in air that travels from the donor animal toward the susceptible animal with some average airflow speed U . An indirect test of transmission mechanism, thus, is to ask: how does the airspeed U affect the probability of transmission?

Intuitively, one expects that, with increasing airspeed (i.e., more air changes per hour), more fresh air is delivered into the test chamber, thus diluting the airborne virus concentration and lowering the probability of transmission. Note that this intuitive analysis, however, is predicated on a key implicit assumption: that the generation rate of aerosolized virus is independent of the airspeed U . This assumption makes sense if expiratory droplets are the main source of aerosolized virus, since the breathing rate and corresponding emission rate of the donor animal are not known to vary appreciably with the speed at which room-temperature air flows past the animal.

This assumption breaks down, however, if aerosolized fomites are an important source of airborne viral counts. In the context of environmental science, it is well established that higher airspeed velocities cause more micron-scale dust to be aerosolized, an effect that plays an important role in soil erosion and air quality [22–25]. Particle resuspension rate from surfaces is known to increase with air swirl velocity [26], and a recent study on human-induced dust resuspension showed that the dust resuspension rate, for example, by walking, increases linearly with airflow rate [27]. This study also suggested that while walking provides the initial energy for dust resuspension, higher speed airflows help keep the particles suspended in the air. In the context of animal models, our previous work showed that dust aerosolization (at a constant airspeed) is highly correlated with animal motion [20,21]. Thus, if higher airspeeds increase the rate of fomite aerosolization and their persistence in the air, or if the animals self-groom or simply move around more in response to higher airspeeds, then the rate at which virus is aerosolized will actually increase with U . In this case the overall transmission probability will not necessarily decrease with U , and potentially could even increase with U , depending on the exact functional dependence between the virus aerosolization rate and the airspeed.

In this paper, we provide a detailed assessment of the impact of airspeed U on the transmission probability of influenza in the guinea pig model. We first assess the classic Wells-Riley model that assumes perfect mixing, as well as a more elaborate Gaussian plume model, to establish a

theoretical framework for the impact of U on transmission probability. We then report experimental measurements of influenza transmission probability between guinea pigs over a wide range of airspeeds. The key finding is that the experimentally observed transmission probability actually increased slightly, from 71% to 78%, when the airspeed was increased by a factor of ten. We interpret this observation as evidence that aerosolized fomites play a nonnegligible role in influenza transmission in the guinea pig model.

II. THEORY

The main goal of this section is to develop a theoretical prediction for how the airspeed U affects the probability of airborne disease transmission between an infected animal and a susceptible animal, as sketched in Fig. 1. Towards that end, we consider two limiting cases: the classic Wells-Riley model, which assumes the air is perfectly well mixed, and a Gaussian plume model, which is more complicated but considers the directionality of the airflow. In both cases, the key result is that increase in the airspeed should substantially decrease the transmission probability, provided one assumes virus aerosolization rate is independent of the airspeed.

A. The Wells-Riley model

The simplest quantitative theoretical model for airborne disease transmission is the Wells-Riley model, named after the early investigators who performed pioneering analyses [28,29]. The Wells-Riley model has been reviewed in detail elsewhere [30,31]; the most important assumption is that the air in the room is perfectly well mixed, so that the relative positions of the infected and susceptible individuals are irrelevant. The final result is that the probability of transmission follows the complement of a Poisson distribution,

$$P = 1 - e^{-\mu}, \quad (1)$$

where μ is the expected number of infectious pathogens that the susceptible individual inhales, defined as

$$\mu = \frac{\eta q B}{Q} t. \quad (2)$$

Here q is the rate, in pathogens per second, at which pathogens are emitted into the air, t is the total exposure time, B is the minute ventilation of the susceptible individuals (i.e., the liters per minute of air exchanged through the lungs), and Q is the room ventilation rate in liters per minute of fresh (pathogen-free) air being delivered to the room. The parameter η here represents an infection efficiency ($0 < \eta < 1$) that encompasses physical effects, like the particle-size-dependent deposition efficiency within the respiratory tract of the susceptible individual [32,33], and immunological effects, like the ability of the immune system to repress the infection [34]. (Note that often η is implicitly assumed to be 1 and these efficiencies are instead wrapped into q , which is defined as a “quanta generation” rate combining both the virus emission into the air and the likelihood of infection upon inhalation.) As μ approaches zero, the transmission probability approaches zero; as μ becomes larger, the transmission probability approaches 1. The probability distribution presented here assumes only one pathogen is necessary to trigger infection; more complicated expressions are available to account for larger minimum infectious doses [35].

Inspection of Eq. (2) illustrates key effects. The expected value and corresponding transmission probability increase with exposure time and with the virus generation rate, which makes sense: more virus or more exposure increases transmission risk. Conversely, increasing the room ventilation rate Q decreases the expected value and corresponding transmission probability; in other words, more fresh air decreases transmission risk. The parameters η and B also affect transmission probability, but these are not readily varied experimentally for a specific virus and animal species; nor would we expect them to vary with airflow speed, as they are parameters mainly reflecting intrahost physiology that should be independent of the external airflow around the host.

To satisfy conservation of mass for the incompressible airflows of interest here, the ventilation rate Q is related to the average airspeed U as

$$Q = UA, \quad (3)$$

where A is the cross-sectional area of the room in the direction orthogonal to the direction of flow. For the sake of completeness, we note that U is also related to the air changes per hour as

$$ACH = \frac{Q}{V} = \frac{UA}{WA} = \frac{U}{W}, \quad (4)$$

where $V = WA$ is the volume of the enclosed space with overall width W .

Combining Eqs. (2) and (3) into (1) yields the desired transmission probability,

$$P = 1 - \exp\left(-\frac{\eta q B}{UA}t\right). \quad (5)$$

We emphasize that this result pertains when the air is well mixed between both animal cages, which is unlikely for the experimental configuration sketched in Fig. 1. Nevertheless, Eq. (5) provides some theoretical insight: the expected value decreases inversely with airspeed U , so the probability necessarily decreases at higher airspeeds, provided the other parameters remain unchanged.

As a thought exercise, we can now ask, ‘‘What must change to keep the observed transmission probability unaltered in response to increased airspeed?’’ If the exposure time and room geometry are held constant, and if the infection efficiency η and pulmonary breathing rate B are both independent of the airspeed, then the only other free parameter is the virus aerosolization rate q . Typically, q is implicitly assumed to result only from expiratory particles, but nothing in the Wells-Riley model necessitates this assumption; all that matters is that virus is aerosolized into the air in some form. In other words, for P to remain constant in response to an increase in airspeed U , the virus aerosolization rate q must increase in direct proportion. This type of relationship has not been previously considered in the airborne disease literature, since there is little reason to expect the ambient airflow will appreciably affect the rate at which an infected individual emits infectious expiratory particles. As discussed below, however, our experimental results suggest that the virus aerosolization rate with guinea pigs indeed increases with the airspeed.

B. The Gaussian plume model

Before turning to our experimental results, we first extend our theoretical consideration by assessing how the directionality of the airflow affects the transmission probability. Unlike in the Wells-Riley model, consideration of the average airflow direction requires information about the relative positions of the infected and susceptible animals. In one limiting case, if the susceptible animal is upwind of the infected animal (i.e., the airspeed direction is reversed in Fig. 1), then it doesn’t matter how much virus is emitted by the infected animal: a sufficiently strong airspeed carries all of the virus-laden particles in the opposite direction away from the susceptible animal, and the transmission probability is zero. If the airflow is directed toward the susceptible animal, however, then the situation is more complicated and details about the nature of the flow must be specified.

This effect of the airflow direction was considered in detail by Halloran *et al.*, who developed a Gaussian plume model to predict the transmission probability [36]. Named ‘‘Gaussian’’ because the time-averaged cross-sectional concentration profile of the plume at any distance downwind from a point source follows a Gaussian (normal) distribution, the nature of Gaussian plumes is well established in the context of emission of pollutants at atmospheric length scales (e.g., from smokestacks [37]). Work with smoke tracing experiments has confirmed that Gaussian plumes also occur at the smaller length scales relevant to animal disease transmission experiments [38]. Full details of the theoretical modeling, including viral growth and decay kinetics and transformation

of the aerosols due to ambient environmental conditions, are presented by Halloran *et al.*; here we focus on a simplified model to elucidate specifically the influence of the average airspeed U .

In the Gaussian plume approach, we again treat the infected individual as a point source of aerosolized pathogens emitted at a rate q . Although animals are free to move around in their cages, we imagine that on average they maintain a separation distance d . As before, our goal is to calculate the transmission probability, which is assumed to follow the Poisson distribution given in Eq. (1). The expected value for the number of infectious pathogens inhaled by the susceptible animal, however, depends on the nature of the airflow. There are two key airflow characteristics: the average airspeed U in the downstream x direction, and the transverse turbulent velocity in the flow, which governs the widths σ_y and σ_z of the plume in the y and z directions orthogonal to the flow. The resulting expected value of pathogens as a function of position due to a slender Gaussian plume is then

$$\mu = \frac{q}{2\pi U \sigma_y \sigma_z} \exp\left(-\frac{y^2}{\sigma_y^2} - \frac{z^2}{\sigma_z^2}\right) \eta B t. \quad (6)$$

For simplicity, here we omit corrections in the pathogen concentration profile due to absorption or reflection on walls, valid for sufficiently small separations. Importantly, the plume widths depend sensitively on downstream position x and are related to the effective turbulent velocity u_y in the direction orthogonal to the flow. For fan-generated airflows, Halloran *et al.* [37] demonstrated that the plume width is independent of the average airspeed, indicating that the effective turbulent velocity is linearly proportional to the average airspeed U . The plume widths thus vary as

$$\sigma_y = \sigma_z = \sqrt{\frac{u_y}{U} \ell x} = \sqrt{k \ell x}, \quad (7)$$

where ℓ is a characteristic eddy length scale set by the fan size and k is a dimensionless constant, on the order of 0.2 to 0.3, that depends on the fan type independent of its speed. Substitution of this turbulent plume width into Eq. (6), and restricting attention to susceptible animals placed directly downstream from the infected individual (i.e., $y = z = 0$ and $x = d$), we obtain the final desired expression

$$P = 1 - \exp\left(-\frac{\eta q B}{2\pi U k \ell d} t\right). \quad (8)$$

Note that this predicted transmission probability is almost identical to that obtained with the Wells-Riley model, except that the cross-sectional area A in Eq. (5) is replaced by the quantity $2\pi k \ell d$. Increasing the airspeed has the same consequence in the Gaussian plume model as for the Wells-Riley model, with the expected value varying inversely with U . A new key conclusion is that the farther the animals are from each other on average, the lower the predicted transmission probability; this decrease occurs because the pathogens have more opportunity to spread laterally the further the animals are from each other, thus decreasing the quantity of pathogens available to be inhaled by the susceptible animal. We note briefly that this approximate analysis omitted the influence of the walls and is thus restricted to sufficiently small values of d such that the plume width is small compared to the height or depth of the cages; a different analysis will pertain if the animals are separated along an extremely long tunnel.

In regard to Eq. (8), we can again ask the question, how do we keep the transmission probability constant as we increase the airspeed? Importantly, the quantities k and ℓ depend on the fan type, not its speed, so the only new possibility compared to the previous analysis is that as U increases, one could in principle force the animals into closer proximity, i.e., decrease d . If, as is customary, the experimental configuration precludes large changes in d , then the Gaussian plume model yields the same conclusion as the Wells-Riley model: to maintain a constant transmission probability while increasing airspeed, the virus aerosolization rate must also increase with airspeed.

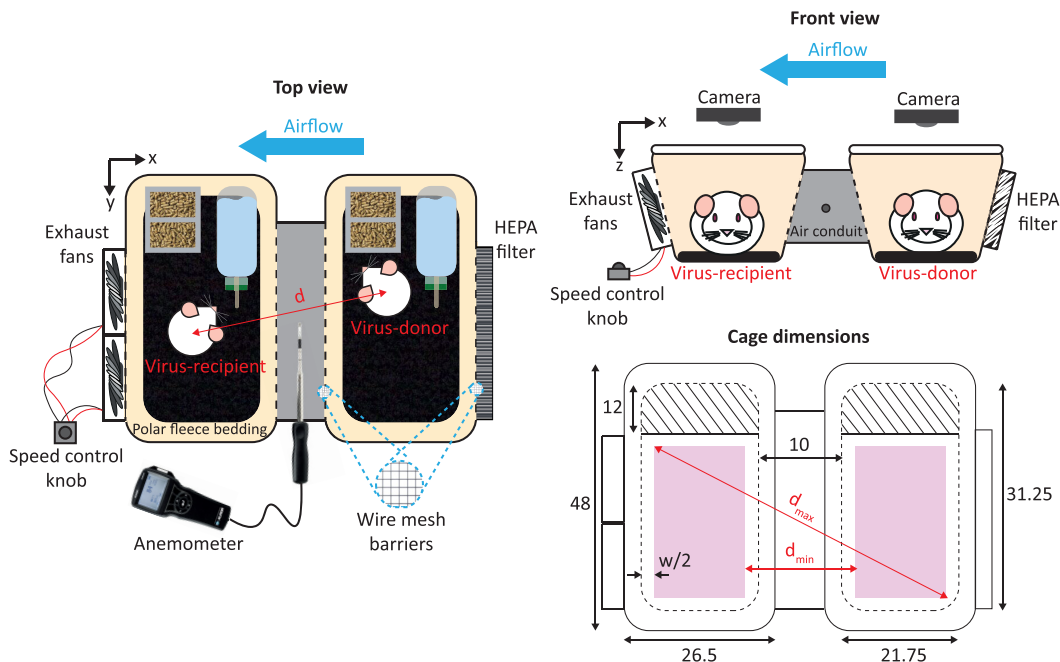


FIG. 2. Custom-fabricated, variable-fan-speed transmission cages. Top view and front view: two animal cages were attached together by a stainless-steel air conduit. Wire mesh barriers were used to close off both sides of the air conduit to prevent contact between animals. A HEPA filter and two CPU fans connected to a speed control knob were used to generate a unidirectional airflow from donor animal to recipient animal cage. Mean airflow speed was measured by an anemometer (averaged over 20-s intervals) in the middle of the cage unit throughout the transmission experiments. Two wide-angle webcam cameras recorded the location of the guinea pigs at 1 image/s. Cage dimensions: all numbers are in centimeters. Dashed lines show the cage floor area (31.25 cm \times 21.75 cm) that is used to calculate the minimum and maximum distance possible between guinea pig centroids ($d_{\max} = 48.4$ cm and $d_{\min} = 20$ cm). Pink areas show all possible locations for the centroid of guinea pigs in the cage considering the approximate guinea pig width of $w = 10$ cm. The hatch pattern shows the area occupied by food and water on the cage floor.

III. METHODS

A. Experimental apparatus

Influenza transmission experiments were performed in a custom-fabricated cage unit used in our previous work [20]. In brief, the cage unit (Fig. 2) consists of two standard polycarbonate animal cages (single cage floor area = 41.25 cm \times 21.75 cm) joined together by a stainless-steel air conduit (width = 10 cm). Note that the cages are large enough in theory to allow for a wide range of possible transmission probabilities, depending on whether the animals tend to reside such that they are separated by d_{\min} or d_{\max} ; using Eq. (6) with appropriate parametric estimates ($U = 0.25$ m s^{-1} , $\ell = 0.06$ m, $k = 0.2$, $\eta = 0.5$, $B = 4.4 \times 10^{-6}$ m³/s, $q = 5 \times 10^{-2}$ s⁻¹, and $t = 4$ days) suggests that $P \approx 0.99$ if the animals remain positioned at d_{\min} , while $P \approx 8.5 \times 10^{-4}$ if they remain positioned at d_{\max} . In practice, however, the guinea pigs are free to move around their cages and thus sample a wide variety of displacements, a quantity that we measured carefully (as discussed below).

For each transmission experiment, one donor animal (guinea pig) intranasally inoculated with influenza virus [Influenza A/Panama/2007/1999 (H3N2) virus (Pan99)] was paired with a virus-naïve recipient. Two adjustable CPU fans drew the air into the unit in a unidirectional manner

through a HEPA filter mounted over the air intake aperture in the cage housing the donor animal. A speed controller knob was used to adjust the airflow speed from a minimum of 0.25 m s^{-1} to a maximum of 2.5 m s^{-1} . This higher velocity corresponds to a “light breeze” (level 2 on the Beaufort scale) and thus is gentle compared to common outdoor conditions that humans experience; with room-temperature air no wind-chill effects occur at this airspeed. A hot-wire anemometer probe measured and recorded airflow velocity, temperature, and relative humidity in the center of the air conduit. In some experiments the fan was deactivated, yielding an average airspeed below the limit of resolution of the anemometer; this small airspeed is described henceforth as ostensibly zero. Wire mesh barriers were used to close off both sides of the air conduit and in front of the fans and HEPA filter to prevent the guinea pigs from having direct contact with each other or touching the fans and filter. Black polar fleece-covered absorbent pads were used as cage bedding, and guinea pig chow and water were also supplied in each cage.

B. Transmission experiments

We performed a total of 40 transmission experiments, with a total of 80 animals, at various airspeeds. All experiments were performed in strict accordance with the recommendations in the Guide for the Care and Use of Laboratory Animals [39], and the research protocol was approved by the Icahn School of Medicine at Mount Sinai Institutional Animal Care and Use Committee (IACUC protocol no. 2014-0178). For each transmission experiment, a guinea pig was intranasally inoculated on day 0, and then placed into the donor (upwind) compartment of a transmission cage unit, prior to placing an influenza virus-naive guinea pig into the recipient (downstream) compartment. Recipient guinea pigs were kept in a separate room in the animal vivarium during inoculation, and gloves were changed before handling the recipient guinea pigs to place them into the transmission cage unit. Transmission pairs were kept together for a total of eight days. Nasal washing was performed on days 2, 4, 6, and 8 or on days 1, 2, and 3 postinoculation (due to limits on anesthesia) for donor animals to confirm infection in intranasally inoculated animals, and on days 2, 4, 6, and 8 for recipient animals to confirm airborne transmission of the influenza virus. Details of the procedures used for influenza virus culture, animal intranasal inoculation, and nasal washing are provided elsewhere [20].

C. Image acquisition and analysis

An ultra-wide-angle web camera mounted above the solid Plexiglas lid of each transmission cage recorded guinea pig locations at one image per second. Red LED lights were used to illuminate the cages during the dark cycle of animal facility. Custom code, written in MATLAB (MathWorks), identified the guinea pig centroids in each time-lapse image and calculated the guinea pig’s instantaneous velocity by quantifying displacement in the centroid coordinates over each 1-s interval. With 40 transmission experiments in total, each with duration between six to eight days, we collected and analyzed a total of 17 654 418 experimental images.

D. Statistics

Our initial intent was to perform equal numbers of trial replicates at each tested airspeed, but preliminary results indicated no sizable difference in transmission probability over the entire range of airspeeds. We then focused on increasing the sample size and corresponding statistical power for the two extreme values of airspeed. Ultimately, 14, 18, 2, 2, and 4 trial replicates were performed at 0.25 m s^{-1} , 2.5 m s^{-1} , 1.75 m s^{-1} , 1 m s^{-1} , and 0 m s^{-1} (fan deactivated), respectively. Bayesian methods were employed to estimate the posterior 95% probability intervals for Pan99 transmission at different airspeeds. With the R packages *rjags* [40,41], *runjags* [42], and *HDInterval* [43], an agnostic beta prior (shape parameters $A = 1$ and $B = 1$) and a Bernoulli likelihood function were used to obtain a 95% credible interval for the posterior distribution of the transmission probability P^{42} given each of these data sets. We used two-sample Kolmogorov-Smirnov (KS) test to compare

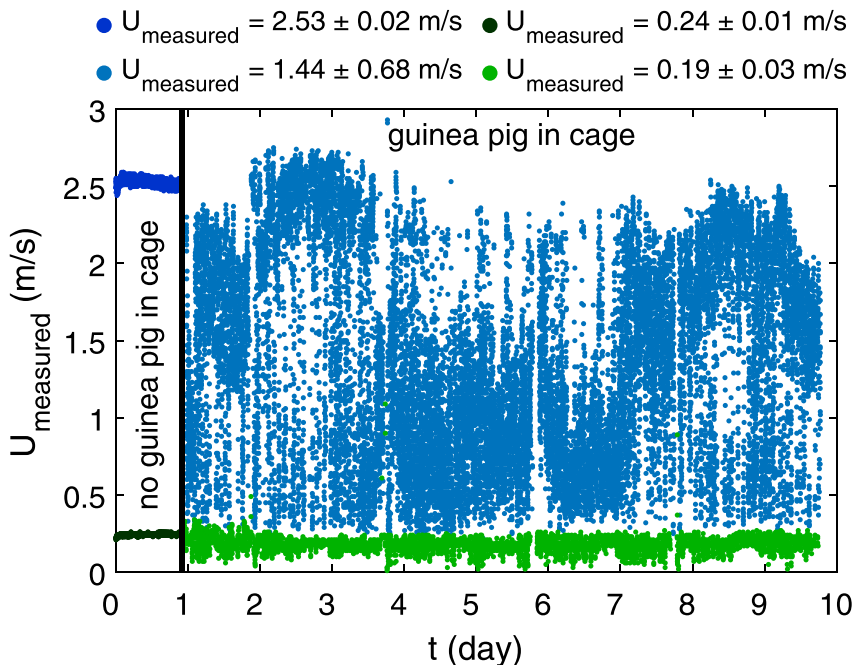


FIG. 3. Representative airflow speed vs time. The airflow velocity was measured between the donor and recipient animal cages using a data logging anemometer at two different fan speeds. The first 22-h measurements were performed before placing the guinea pigs in the cages, and the measurements continued after placing the guinea pigs in the cages until the end of transmission experiments. Fluctuations in airspeed are due to animal motion in front of the sensor.

the (non-Gaussian) histograms of the instantaneous distance between guinea pigs and to compare histograms of their respective instantaneous velocities. The KS test is a nonparametric test that evaluates the difference between cumulative distribution functions of two samples; specifically, it rejects the null hypothesis that the data of two samples are drawn from the same continuous distribution if $P > \alpha$, where $\alpha = 0.05$ is the significance level.

IV. RESULTS

Our measurements with an anemometer confirmed that the average airspeed remained within a few percent of the ostensible airspeed over the course of each multiday transmission experiment (Fig. 3). At the ostensible speed of 0.25 m s^{-1} and 2.5 m s^{-1} , the actual airspeed was measured as $0.24 \pm 0.01 \text{ m s}^{-1}$ and $2.53 \pm 0.02 \text{ m s}^{-1}$, respectively for 22 h before placing the guinea pigs in the cage. After placing the guinea pigs inside the cages, fluctuations increased primarily because of animal motion in front of the sensor, with the highest fluctuations for 2.5 m s^{-1} speed as expected. Simultaneous temperature and humidity measurements confirmed that the ambient conditions inside the environmental chamber remained constant through all experiments at approximately 20°C and 25% relative humidity. No qualitative differences were observed in food or water consumption, nor fecal pellet production, at any airspeed.

The viral titer dynamics for all animals placed in either low or high airspeed are shown in Fig. 4. As expected, all intranasally inoculated donor animals became infected and exhibited viral titer dynamics that began near zero, increased to a peak of near 10^7 PFU/ml at 2 to 3 days post-inoculation (dpi), and then decayed by 4 dpi. These observed dynamics are similar to prior

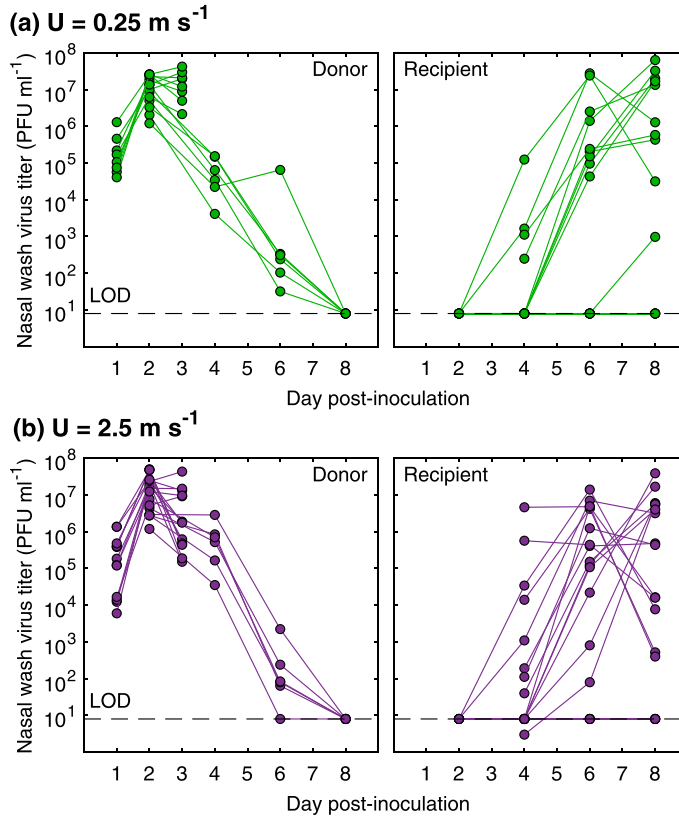


FIG. 4. Nasal wash titers for donor and recipient guinea pigs. Nasal wash titers for the donor and recipient guinea pigs for average airflow speed (a) $U = 0.25 \text{ m s}^{-1}$ (10 out of 14 infected), and (b) $U = 2.5 \text{ m s}^{-1}$ (14 out of 18 infected).

observations with this same animal model and virus [9,10]. No appreciable difference is noted in the viral titer dynamics of the donor animals at any airspeed tested.

Under the experimental conditions, large fractions of the susceptible animals became infected. At the low airspeed of $U = 0.25 \text{ m s}^{-1}$ [shown in Fig. 4(a)], a total of four susceptible animals exhibited viral titers above the limit of detection by day 4, another five by day 6, and one more by day 8. No virus above the limit of detection was observed in the remaining four animals at any time point. In all, 10 of the 14 susceptible animals (71%) were infected at the low airspeed. At the high airspeed of $U = 2.5 \text{ m s}^{-1}$ [shown in Fig. 4(b)], a total of seven susceptible animals exhibited viral titers above the limit of detection by day 4, and another seven by day 6. No virus above the limit of detection was observed in the remaining four animals at any time point. In all, 14 of the 18 susceptible animals (78%) were infected at the higher airspeed.

The transmission data in Fig. 4 are summarized in Fig. 5, which shows the observed transmission probability and corresponding 95% credible intervals vs airspeed. For the sake of completeness, we also include our preliminary experiments performed with zero fan speed and intermediate fan speeds, though they lack a comparable amount of statistical power. The most important trend observed is that the transmission probability varied little with airspeed, where the most important result is the direct comparison between 0.25 and 2.5 m s^{-1} . At the lower airspeed of 0.25 m s^{-1} , the 71% transmission probability has a 95% credible range of 47% to 89%. In contrast, at the higher airspeed of 2.5 m s^{-1} , the 78% transmission probability has a 95% credible range of 56% to 92%. Using the Fisher's exact test yields a Pearson's P value of 0.704, indicating that we are unable to

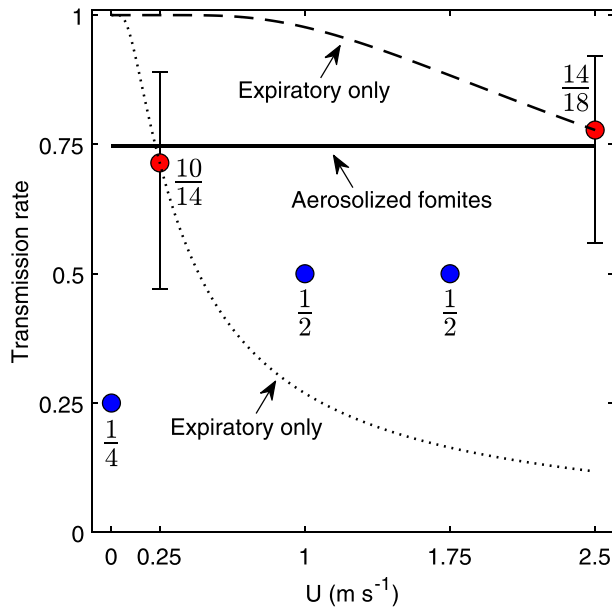


FIG. 5. Cumulative transmission rate vs average airflow speed. Error bars show the 95% confidence intervals for 0.25 m s^{-1} and 2.5 m s^{-1} average airflow speeds. Fractional numbers next to each data point shows the transmission rate as (number of cases that transmission occurred at a specific airflow speed/total number of cases at that speed). The dotted line is the transmission rate values calculated using either Eqs. (5) or (8) and experimentally observed probability of 71% at 0.25 m s^{-1} to estimate other model parameters. Similarly, the transmission rate values shown with the dashed line are calculated using experimentally observed probability of 78% at 2.5 m s^{-1} to estimate other model parameters. The solid line is the probability of transmission calculated based on either Eqs. (11a) or (11b) to calculate other model parameters. Red markers denote airflow speeds where statistically significant sample sizes of animal pairs were tested; blue markers denote nonstatistically significant sample sizes but are included for completeness. Confidence intervals are omitted for blue data points due to their small sample size.

reject the null hypothesis that the transmission probability is significantly different at these two airspeeds. In other words, increasing the airflow by a factor of ten had no statistically significant impact on the transmission rate.

Recalling that the Gaussian plume model indicates that the relative positions of the animals could affect the probability of transmission, a potential explanation is that at the higher airspeeds the animals for some reason tended to be closer to each other and thus inhaled larger concentrations of aerosol particles carrying virus. Our video recordings of the relative positions of each animal pair do not corroborate this hypothesis.

Figure 6 shows the cumulative location heatmaps for the infected and susceptible animals during the transmission experiments based on the percentage of time that the animal centroid resided at a specific location, integrated over the entire eight-day transmission experiment. This representation provides a qualitative overview of where the animals tended to position themselves and could have revealed that animals that transmitted the virus tended to reside on the same side of the cage, while animals that did not transmit the virus tended to reside in opposite corners. No such trend is observed. Instead, for both average velocities tested here ($U = 0.25 \text{ m s}^{-1}$ and $U = 2.5 \text{ m s}^{-1}$), the heatmaps reveal there is no apparent systematic difference between the location of guinea pigs for the cases that the susceptible animal became infected [Figs. 6(a) and 6(c)] vs the cases that the virus did not transmit [Figs. 6(b) and 6(d)]. In other words, there is no obvious way to differentiate the heatmaps based on the positioning of the hotspots.

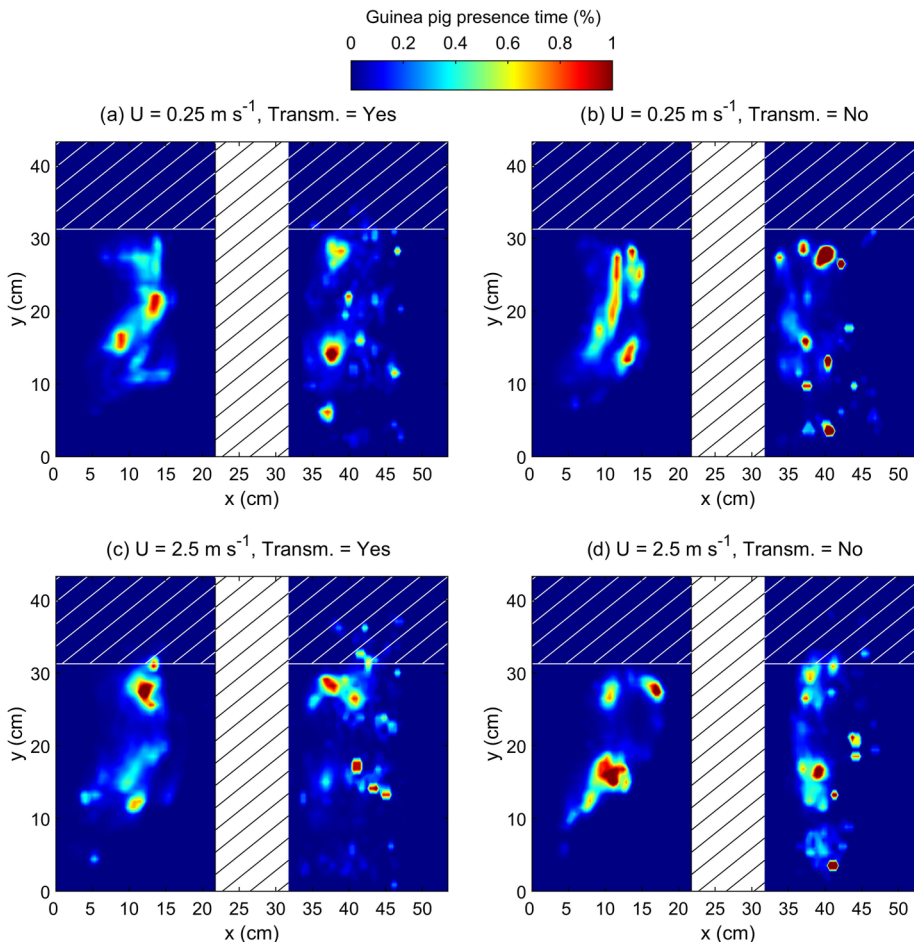


FIG. 6. Cumulative location heatmaps. Animal centroids, integrated over eight days for infected (right cage) and susceptible (left cage) guinea pigs placed inside the cage unit shown in Fig. 2, for the cases that virus-naïve recipients became infected (Transm. = Yes) at (a) $U = 0.25 \text{ m s}^{-1}$ and (c) $U = 2.5 \text{ m s}^{-1}$ and for the cases that influenza virus did not transmit (Transm. = No) at (b) $U = 0.25 \text{ m s}^{-1}$ and (d) $U = 2.5 \text{ m s}^{-1}$. The white hatch pattern shows the location of food and water in the cages, and the black hatch pattern shows the air conduit separating the infected and susceptible guinea pig cages.

The heatmaps show the preferred positions, but since they are time integrated they provide no information about the instantaneous relative positions. To further assess how the respective locations of the animals might have affected the transmission, we analyzed the instantaneous distance between the animals. Figure 7 shows histograms of the instantaneous downstream distance between animals, $\Delta x = x_{\text{donor}} - x_{\text{recipient}}$ (top row), their instantaneous cross-flow separation distance, $\Delta y = y_{\text{donor}} - y_{\text{recipient}}$ (middle row), and the overall Cartesian distance between the guinea pigs $d = (\Delta x^2 + \Delta y^2)^{1/2}$, separated out for pairs where transmission occurred or did not occur and by airflow speed. Note that the air conduit width between two animal cages is 10 cm, but since we define the guinea pig's location as its centroid, and with an average width of approximately 10 cm for the guinea pigs themselves, the minimum and maximum possible distance between the animals is $\approx 20 \text{ cm}$ and $\approx 48.4 \text{ cm}$, respectively. All of the Δx and d distributions to good approximation are normal (Gaussian). In contrast, the Δy distributions are more trimodal, reflecting the positioning

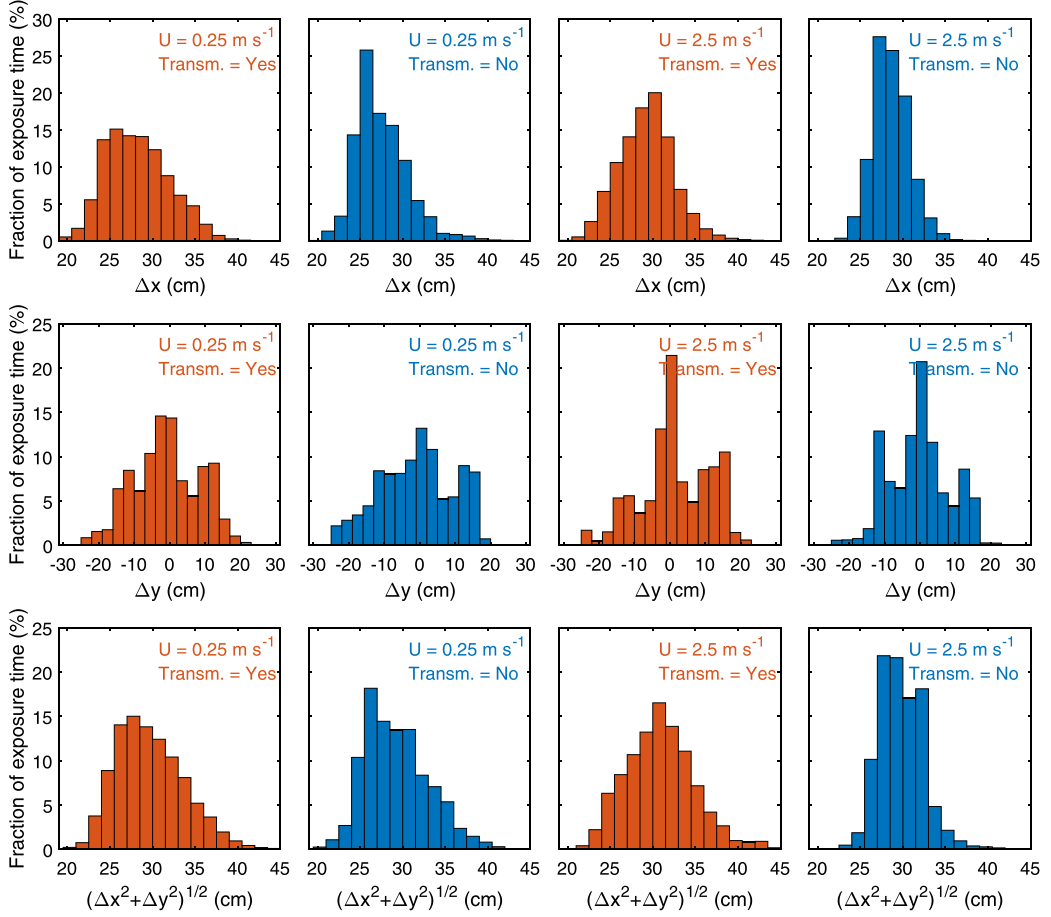


FIG. 7. Histograms of instantaneous animal separation. Top row: downstream distance between the animals $\Delta x = x_{\text{donor}} - x_{\text{recipient}}$. Middle row: cross-flow separation distance between the animals $\Delta y = y_{\text{donor}} - y_{\text{recipient}}$. Bottom row: Cartesian distance between the animals $d = (\Delta x^2 + \Delta y^2)^{1/2}$. In each row, histograms are separated for average airflow speed of $U = 0.25 \text{ m s}^{-1}$ (left) and $U = 2.5 \text{ m s}^{-1}$ (right), and further separated by whether the virus-naive recipients became infected (red histograms) or did not become infected (blue histograms). None of the respective distribution pairs are statistically significantly different (cf. Table I).

TABLE I. Two-sample Kolmogorov-Smirnov test results comparing the displacement histograms shown in Fig. 7. N is the sample size, i.e., the number of images each histogram is based on.

	0.25 m s^{-1} vs 2.5 m s^{-1}		Transmission vs no Transmission	
	Transmission	No transmission	0.25 m s^{-1}	2.5 m s^{-1}
N	4 891 817 vs 6 203 465	1 534 518 vs 2 268 621	4 891 817 vs 1 534 518	6 203 465 vs 2 268 621
P value				
Δx	0.99	0.19	0.93	0.19
Δy	0.63	0.63	0.91	0.91
d	0.99	0.6	0.99	0.4

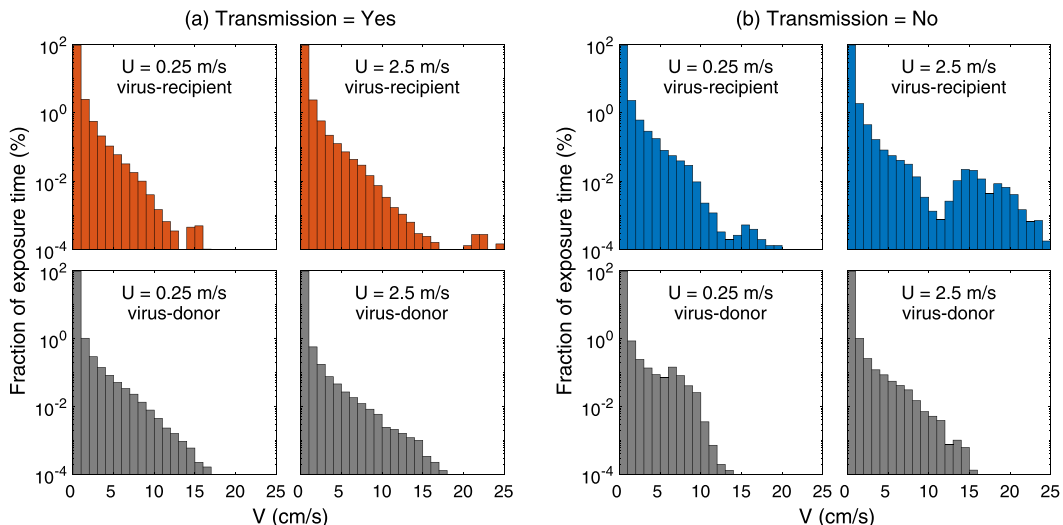


FIG. 8. Histograms of instantaneous animal velocity. Fraction of exposure time vs instantaneous guinea pig movement velocity, defined as $V = d[(\Delta x^2 + \Delta y^2)]/dt$ averaged over 1-s increments. Cumulative results for average airflow speed of $U = 0.25 \text{ m s}^{-1}$ or $U = 2.5 \text{ m s}^{-1}$ when virus-naive recipient (a) became infected or (b) did not become infected. Note the vertical scales are logarithmic. See Table II for the results of two-sample Kolmogorov-Smirnov test.

of the food and water supply on only one side of the cage (see Fig. 2); the smaller peaks near $\pm 15 \text{ cm}$ represent when one animal was feeding while the other was on the far side of their cage. Most importantly, there are no apparent statistically significant differences between the Δx , Δy , or d distributions for the cases of transmission vs no transmission for both $U = 2.5 \text{ m s}^{-1}$ and $U = 0.25 \text{ m s}^{-1}$. As shown in Table I, the P values based on a two-sample Kolmogorov-Smirnov test range from 0.19 to 0.99, all much larger than $\alpha = 0.05$. In other words, the animals tended to move about in their cages randomly, with no apparent differences depending on whether the airspeed was large or small or whether they became infected. We conclude from these data that no significant differences in the relative positions of the animals occurred between the different experimental conditions.

Finally, to further test for any systematic differences in the behavior of the guinea pigs, we prepared histograms showing the fraction of total exposure time vs the instantaneous guinea pig movement velocity, defined as $V = \frac{d}{dt}(\Delta x^2 + \Delta y^2)$ averaged over 1-s intervals (i.e., the same metric presented in our prior work [20]). Figure 8 shows histograms of the fraction of time spent moving at particular velocities. Note that the vertical scales are logarithmic, and the animals spent the vast majority of the time stationary (large peaks near $V = 0$). The key finding is that the infected animals

TABLE II. Two-sample Kolmogorov-Smirnov test results comparing the velocity histograms shown in Fig. 8. N is the sample size, i.e., the number of images each histogram is based on.

		0.25 m s ⁻¹ vs 2.5 m s ⁻¹	
		Transmission	No transmission
	N	4 891 817 vs 6 203 465	1 534 518 vs 2 268 621
P value	Virus recipient	0.12	0.19
	Virus donor	0.99	0.6

were similarly “active” in terms of net displacements in low ($U = 0.25 \text{ m s}^{-1}$) and high ($U = 2.5 \text{ m s}^{-1}$) average airflow speed conditions. Statistical analysis corroborates this observation, with no statistically significant differences in the velocity distributions for any conditions (Table II).

V. DISCUSSION

The key observation is that the transmission probability remained the same despite a tenfold increase in the ventilation airspeed. As discussed in the theory section, both the Wells-Riley model and the Gaussian plume model suggest that increasing the airspeed should decrease the transmission probability. Indeed, we can use the experimentally observed probability of 71% at the lower airspeed to estimate μ as

$$\mu = \ln\left(\frac{1}{1 - 0.71}\right) = 1.24. \quad (9)$$

If we assume all other parameters are held constant but the airspeed increases by a factor of ten [using either Eqs. (5) or (8)], then we would expect $\mu = 0.124$ and the probability at the increased airspeed should be $P = 12\%$. Importantly, this value falls well below the 95% credible interval for the observed 78% probability at the increased airspeed (Fig. 5). Generalization of this calculation for arbitrary increases in airspeed yields the dotted curve in Fig. 5, which undershoots the observed probability significantly. Using a similar approach, if we use the probability of 78% at higher airflow speed of 2.5 m s^{-1} to estimate μ , assuming that all other parameters remain constant, the probability of transmission at 0.25 m s^{-1} will be calculated as $\sim 100\%$, which is well above the upper limit of 95% credible interval for observed 71% probability (Fig. 5, dashed line). We conclude that our assumption is incorrect: some other parameters that comprise μ must also change as the airspeed changes. In the Wells-Riley model, the chamber cross-sectional area A was not changed, and in the Gaussian plume model, the fan parameters k and ℓ are independent of fan speed [37]. Likewise, the histograms in Fig. 7 indicate that no significant change in d or y occurred between different airspeeds. The infection efficiency η reflects the efficiency of physical deposition within the lungs of the susceptible animal, which should not change with the ambient airspeed, as well as the immune system response. Although prolonged exposure to low temperatures is known to affect immune responses [44,45], our experiments were performed at constant room temperature; we are unaware of any evidence that increased ventilation airspeed will have a deleterious effect on mammalian immune systems.

Thus, the only remaining possible parameter that could account for the observations is that the virus aerosolization rate q actually increases with airspeed. In fact, if we hypothesize that the virus aerosolization rate is linearly proportional to the airspeed,

$$q = \gamma U, \quad (10)$$

then by either the Wells-Riley model or the Gaussian plume model we anticipate that the probability is independent of airspeed, in accord with the observations (solid line, Fig. 5). Here γ is a proportionality constant with dimensions of viral particles per meter. Insertion of Eq. (10) into the models derived earlier yields

$$\text{(Wells-Riley)} \quad P = 1 - \exp\left(-\frac{\eta\gamma B}{A}t\right), \quad (11a)$$

$$\text{(Gaussian)} \quad P = 1 - \exp\left(-\frac{\eta\gamma B}{2\pi k\ell d}t\right). \quad (11b)$$

In other words, if the aerosolization rate of virus is linearly proportional to the airspeed as suggested by Eq. (10), then both models yield transmission probability that has no direct dependence on airspeed.

It then remains to assess why the virus aerosolization rate might vary linearly with airspeed. There is no reason to expect that the animal breathing rate or amount of virus emitted via expiratory particles will increase linearly with the surrounding airflow speed. Equation (10) is consistent, however, with an alternative mechanism based on aerosolized fomites. Our prior work also clearly established that intranasally inoculated guinea pigs contaminate their fur, their paws, and their (dusty) cage walls, presumably via self-grooming and direct mouth and nose contact. We further established that the vast majority of aerosol particles (99% or more) traveling from the donor cage to the susceptible cage are nonrespiratory dust, and that virus-contaminated dust particles can transmit viable virus and infect susceptible animals [20]. It is also firmly established in the aerosol science community that higher wind speeds cause more dust to be aerosolized from solid surfaces [26,46]. Indeed, previous work [27] has found that dust resuspension from a floor by a human walking over it is a linear function of the background air speed. Taking these observations together, we conclude that the most plausible explanation for our observations is that virus was carried between the guinea pigs primarily by aerosolized fomites, and that their rate of aerosolization follows Eq. (10).

This interpretation has several far-reaching implications. The guinea pig model described here has been heavily used to investigate influenza [9,11,47,48], and in particular has spurred much research on the effect of ambient temperature and humidity on the transmissibility of influenza virus. For example, high transmission was observed at 5 °C, but zero transmission was observed at 30 °C [10]. This observation has been interpreted primarily in terms of the impact of temperature on either airborne virus survivability, or on the immune response or physiology of the animals. In addition, guinea pigs have been observed both qualitatively [10] and quantitatively [49] to exhibit lethargic behavior at hot temperatures (30 °C) compared to their activity level at room temperature. While the above studies either did not appreciate or did not assess changes in guinea pig activity level at temperatures below room temperature (e.g., 5 °C), it is plausible that ambient cold induces increased activity to generate warmth. Therefore, if aerosolized fomites are the primary mechanism for transmission, there is a much simpler potential explanation for the higher rate of transmission at 5 °C: guinea pigs prefer colder temperatures and are noticeably lethargic at 30 °C. If they don't move much, they won't aerosolize as much dust, and therefore the probability of infecting the susceptible animal decreases. Likewise, the ambient humidity is also known to affect how strongly dust particulates cling to solid surfaces [46]. Changes in the humidity could therefore affect the aerosolization rate and the consequent transmission probability.

The results presented here also raise the question of whether aerosolized fomites play a significant role in other animal models for airborne disease transmission, such as ferrets, mice, and pigs. All animals and their cage environment have aerosolizable dust, and although to date we have little hard data, other animal species are known to contaminate their environment and surrounding dust with influenza [50]. Since animal models are so often used to assess the airborne transmissibility of particular virus strains, additional experiments comparable to those presented here should be conducted with other animal models to help determine the mechanisms of transmission.

A final comment key question is whether aerosolized fomites play a significant role in respiratory viral transmission between humans. Note that standard indoor environments are similar to animal cages in the sense that air is pumped into a space where occupant motion can help aerosolize potentially virus-contaminated particulates. The results presented here establish a quantitative framework for considering this possibility in more detail.

All data are available in the manuscript. MATLAB code for quantifying guinea pig location from time-lapse images is available from the corresponding author upon reasonable request.

ACKNOWLEDGMENT

This research was supported by the National Institute for Allergy and Infectious Diseases (NIAID) of the National Institutes of Health (NIH), Grant No. R01 AI110703 to N.M.B., W.D.R., and A.S.W.

S.A., W.D.R., A.S.W., and N.M.B. designed the transmission cage unit. N.G., R.S.B., and S.A. performed guinea pig experiments, including intranasal virus inoculations, transmission experiments, and collection and titration of nasal washes. A.S.W., W.D.R., and N.M.B. conceived the project, and all authors contributed to experimental design. S.A., W.D.R., and N.M.B. analyzed the data and wrote the manuscript. All authors reviewed and revised the manuscript for accuracy and intellectual content. The authors declare no competing interests.

- [1] R. Karia, I. Gupta, H. Khandait, A. Yadav, and A. Yadav, COVID-19 and its modes of transmission, *SN Compr. Clin. Med.* **2**, 1798 (2020).
- [2] R. Zhang, Y. Li, A. L. Zhang, Y. Wang, and M. J. Molina, Identifying airborne transmission as the dominant route for the spread of COVID-19, *Proc. Natl. Acad. Sci. USA* **117**, 14857 (2020).
- [3] S. Chaudhuri, S. Basu, and A. Saha, Analyzing the dominant SARS-CoV-2 transmission routes toward an ab initio disease spread model, *Phys. Fluids* **32**, 123306 (2020).
- [4] G. Brankston, L. Gitterman, Z. Hirji, C. Lemieux, and M. Gardam, Transmission of influenza A in human beings, *Lancet Infect. Dis.* **7**, 257 (2007).
- [5] R. Tellier, Aerosol transmission of influenza A virus: A review of new studies, *J. R. Soc. Interface* **6**, S783 (2009).
- [6] B. Killingley and J. Nguyen-Van-Tam, Routes of influenza transmission, *Influenza Other Respiratory Viruses* **7**, 42 (2013).
- [7] R. Tellier, Y. Li, B. J. Cowling, and J. W. Tang, Recognition of aerosol transmission of infectious agents: A commentary, *BMC Infect. Dis.* **19**, 101 (2019).
- [8] S. Asadi, N. Bouvier, A. S. Wexler, and W. D. Ristenpart, The coronavirus pandemic and aerosols: Does COVID-19 transmit via expiratory particles? *Aerosol Sci. Technol.* **54**, 635 (2020).
- [9] A. C. Lowen, S. Mubareka, T. M. Tumpey, A. Garcia-Sastre, and P. Palese, The guinea pig as a transmission model for human influenza viruses, *Proc. Nat. Acad. Sci. USA* **103**, 9988 (2006).
- [10] A. C. Lowen, S. Mubareka, J. Steel, and P. Palese, Influenza virus transmission is dependent on relative humidity and temperature, *PLoS Pathog.* **3**, e151 (2007).
- [11] A. C. Lowen, N. M. Bouvier, and J. Steel, Transmission in the Guinea Pig Model, in *Influenza Pathogenesis and Control - Volume I, Current Topics in Microbiology and Immunology*, edited by R. Compans and M. Oldstone (Springer, Cham, 2014), Vol. 385, pp. 157–183, https://doi.org/10.1007/82_2014_390.
- [12] F. Koster *et al.*, Exhaled aerosol transmission of pandemic and seasonal H1N1 influenza viruses in the ferret, *PLoS ONE* **7**, e33118 (2012).
- [13] J. Zhou, J. Wei, K.-T. Choy, S. F. Sia, D. K. Rowlands, D. Yu, C.-Y. Wu, W. G. Lindsley, B. J. Cowling, J. McDevitt *et al.*, Defining the sizes of airborne particles that mediate influenza transmission in ferrets, *Proc. Natl. Acad. Sci. USA* **115**, E2386 (2018).
- [14] J. F. Gritzfeld, P. Roberts, L. Roche, S. El Batrawy, and S. B. Gordon, Comparison between nasopharyngeal swab and nasal wash, using culture and PCR, in the detection of potential respiratory pathogens, *BMC Res. Notes* **4**, 122 (2011).
- [15] T. Heikkinen, J. Marttila, A. A. Salmi, and O. Ruuskanen, Nasal swab versus nasopharyngeal aspirate for isolation of respiratory viruses, *J. Clin. Microbiol.* **40**, 4337 (2002).
- [16] M. Linster *et al.*, Identification, Characterization, and natural selection of mutations driving airborne transmission of A/H5N1 virus, *Cell* **157**, 329 (2014).
- [17] C. Muñoz-Fontela *et al.*, Animal models for COVID-19, *Nature (London)* **586**, 509 (2020).
- [18] M. Richard *et al.*, SARS-CoV-2 is transmitted via contact and via the air between ferrets, *Nat. Commun.* **11**, 3496 (2020).
- [19] S. S. Lakdawala and V. D. Menachery, The search for a COVID-19 animal model, *Science* **368**, 942 (2020).
- [20] S. Asadi *et al.*, Influenza A virus is transmissible via aerosolized fomites, *Nat. Commun.* **11**, 4062 (2020).

- [21] S. Asadi *et al.*, Non-respiratory particles emitted by guinea pigs in airborne disease transmission experiments, *Sci. Rep.* **11**, 17490 (2021).
- [22] Y. Yang *et al.*, Dust-wind interactions can intensify aerosol pollution over eastern China, *Nat. Commun.* **8**, 15333 (2017).
- [23] H. Burezq, Combating wind erosion through soil stabilization under simulated wind flow condition—Case of Kuwait, *Int. Soil Water Conserv. Res.* **8**, 154 (2020).
- [24] H. W. Pi, D. R. Huggins, J. T. Abatzoglou, and B. Sharratt, Modeling soil wind erosion from agroecological classes of the Pacific Northwest in response to current climate, *J. Geophys. Res.—Atmos.* **125**, e2019JD031104 (2020).
- [25] O. Stenz and B. Hor, Wind erosion related dust emissions: Comparison of emission factors determined by ambient air quality measurements with two calculation methods, *Gefahrstoffe Reinhalt. Luft* **80**, 246 (2020).
- [26] P. Salimifard, D. Rim, C. Gomes, P. Kremer, and J. D. Freihaut, Resuspension of biological particles from indoor surfaces: Effects of humidity and air swirl, *Sci. Total Environ.* **583**, 241 (2017).
- [27] Z. Sun, Sh. Zheng, Y. Fu, and M. Chai, Characteristics of indoor human-induced particle resuspension under different ventilation conditions, *Indoor Built Environ.* **31**, 1907 (2022).
- [28] W. F. Wells, Threshold sanitary ventilation, in *Airborne Contagion and Air Hygiene* (Harvard University Press, Cambridge, MA, 1955), pp. 269–299.
- [29] E. C. Riley, G. Murphy, and R. L. Riley, Airborne spread of measles in a suburban elementary school, *Am. J. Epidemiol.* **107**, 421 (1978).
- [30] G. N. Sze To and C. Y. H. Chao, Review and comparison between the Wells-Riley and dose-response approaches to risk assessment of infectious respiratory diseases, *Indoor Air* **20**, 2 (2010).
- [31] C. J. Noakes and P. A. Sleight, Mathematical models for assessing the role of airflow on the risk of airborne infection in hospital wards, *J. R. Soc. Interface* **6**, S791 (2009).
- [32] J. P. Schreider and J. O. Hutchens, Particle deposition in the guinea pig respiratory tract, *J. Aerosol. Sci.* **10**, 599 (1979).
- [33] J. Rissler *et al.*, Deposition efficiency of inhaled particles (15–5000 nm) related to breathing pattern and lung function: An experimental study in healthy children and adults, *Part. Fibre Toxicol.* **14**, 10 (2017).
- [34] D. D. Chaplin, Overview of the immune response, *J. Allergy Clin. Immunol.* **125**, S3 (2010).
- [35] S. Yezli and J. A. Otter, Minimum infective dose of the major human respiratory and enteric viruses transmitted through food and the environment, *Food Environ. Virol.* **3**, 1 (2011).
- [36] S. K. Halloran, A. S. Wexler, and W. D. Ristenpart, A Comprehensive breath plume model for disease transmission via expiratory aerosols, *PLoS ONE* **7**, e37088 (2012).
- [37] I. Ben-Gal, R. Katz, and Y. Bukchin, Robust eco-design: A new application for air quality engineering, *IIE Trans.* **40**, 907 (2008).
- [38] S. K. Halloran, A. S. Wexler, and W. D. Ristenpart, Turbulent dispersion via fan-generated flows, *Phys. Fluids* **26**, 055114 (2014).
- [39] National Research Council, *Guide for the Care and Use of Laboratory Animals*, 8th ed. (National Academics Press, Washington, DC, 2011).
- [40] D. Lunn, D. Spiegelhalter, A. Thomas, and N. Best, The BUGS project: Evolution, critique and future directions, *Stat. Med.* **28**, 3049 (2009).
- [41] M. Plummer, N. Best, K. Cowles, and K. Vines, CODA: Convergence diagnosis and output analysis for MCMC, *R News* **6**, 7 (2006).
- [42] M. J. Denwood, runjags: An R package providing interface utilities, model templates, parallel computing methods and additional distributions for MCMC models in JAGS, *J. Statist. Softw.* **71**, 1 (2016).
- [43] J. K. Kruschke, *Doing Bayesian Data Analysis: A Tutorial with R and BUGS* (Elsevier, Amsterdam, 2011).
- [44] R. J. Shephard and P. N. Shek, Cold exposure and immune function, *Can. J. Physiol. Pharmacol.* **76**, 828 (1998).
- [45] M. Moriyama and T. Ichinohe, High ambient temperature dampens adaptive immune responses to influenza A virus infection, *Proc. Nat. Acad. Sci. USA* **116**, 3118 (2019).
- [46] I. Goldasteh, G. Ahmadi, and A. Ferro, Effect of air flow on dust particles resuspension from common flooring, in *Proceedings of the ASME 2010 3rd Joint US-European Fluids Engineering*

- Summer Meeting collocated with 8th International Conference on Nanochannels, Microchannels, and Minichannels, Volume 1, Symposia – Parts A, B, and C. Montreal, Quebec, Canada. August 1–5, 2010, Fluids Engineering Division Summer Meeting (American Society of Mechanical Engineers, Canada, 2010), pp. 2797–2800, <https://doi.org/10.1115/FEDSM-ICNMM2010-30596>.*
- [47] N. M. Bouvier and A. C. Lowen, Animal models for influenza virus pathogenesis and transmission, *Viruses* **2**, 1530 (2010).
- [48] N. M. Bouvier, Animal models for influenza virus transmission studies: A historical perspective, *Curr. Opin. Virol.* **13**, 101 (2015).
- [49] E. E. Nicholls, A study of the spontaneous activity of the guinea pig, *J. Comp. Psychol.* **2**, 303 (1922).
- [50] D. G. F. Edward, Resistance of influenza virus to drying and its demonstration on dust, *Lancet* **2**, 664 (1941).